CSIRO PUBLISHING

COLLECTION | RESEARCH PAPER
https://doi.org/10.1071/WF24225

International Journal of WILDLAND FIRE
International Association of Wildland Fire

Predicting potential postfire debris-flow hazards across California prior to wildfire

Rebecca K. Rossi[A,*], Paul W. Richardson[B], David B. Cavagnaro[A], Stefani G. Lukashov[A], Mary Ellen Miller[C] and Donald N. Lindsay[B]

For full list of author affiliations and declarations see end of paper

***Correspondence to:**
Rebecca K. Rossi
California Geological Survey, Burned Watershed Geohazards Program, Sacramento, CA 95814, USA
Email: rebecca.rossi@conservation.ca.gov

Received: 21 December 2024
Accepted: 26 May 2025
Published: 3 July 2025

Cite this: Rossi RK *et al.* (2025) Predicting potential postfire debris-flow hazards across California prior to wildfire. *International Journal of Wildland Fire* **34**, WF24225. doi:10.1071/WF24225

© 2025 The Author(s) (or their employer(s)). Published by CSIRO Publishing on behalf of IAWF.
This is an open access article distributed under the Creative Commons Attribution-NonCommercial-NoDerivatives 4.0 International License (CC BY-NC-ND)

OPEN ACCESS

ABSTRACT

Background. Wildfires and consequent postfire hazards, specifically runoff-generated debris flows, are a major threat to California communities. **Aim.** To help prefire planning efforts across California, we identified areas that are most susceptible to postfire debris flows before fire occurs. **Methods.** We developed a calibration method for an established model that relates existing vegetation type to fire severity, a critical input to the US Geological Survey's postfire debris-flow likelihood model. We calibrated the model for eight regions with data from 81 wildfires that occurred in 2020 and 2021 in California. **Key results.** We predicted debris-flow likelihood, volume, and combined hazard classification, and created statewide maps that use simulated fire frequency and rainfall data to predict the probability that a basin will experience a wildfire and subsequent debris flow. **Conclusions.** We suggest that the model predictions are useful for identifying areas that pose the greatest risk of postfire debris-flow hazard for a simplified wildfire scenario. **Implications.** Although actual patterns of wildfire severity may vary from our simulated products, we show that applying a consistent methodology for all of California is useful for identifying areas that are likely to pose the greatest postfire hazards, which should help focus prefire mitigation efforts.

Keywords: annual probability of postfire debris flow, California wildfires, existing vegetation type, geohazards, postfire debris flows, prefire hazard mitigation, risk assessment, runoff-generated debris flow, simulated burn severity, simulated fire, statewide prefire planning.

Introduction

Since the 1980s, California wildfires have increased in number, size, and severity, resulting in significant impacts to the environment, economy, and society (Li and Banerjee 2021). This is particularly evident in the past two decades where 18 of the 20 largest wildfires in California history have occurred since 2000, and where 15 of the 20 most costly and destructive fires to property in the state have occurred since 2015 (California Department of Forestry and Fire Protection 2024). Factors influencing the frequency, size, and destructiveness of wildfires include droughts and rising temperatures aggravated by climate change, as well as fire suppression, land management policies, and human encroachment into wildlands (Radeloff *et al.* 2018; Belongia *et al.* 2023).

One of the more impactful postfire hazards in California are runoff-generated debris flows that frequently occur within 3 years following fire and can damage ecosystems, critical infrastructure, and pose a risk to life safety within and downgradient of the burned area (e.g. Kean *et al.* 2019; Thomas *et al.* 2023; Zekkos and Stark 2023; Rundio *et al.* 2024; Swanson *et al.* 2024). Emergency managers, road and critical facility engineers, and flood control district officers are often challenged with little time to design and construct mitigation measures or develop and implement postfire response and evacuation plans

Collection: Establishing Directions in Postfire Debris-Flow Science

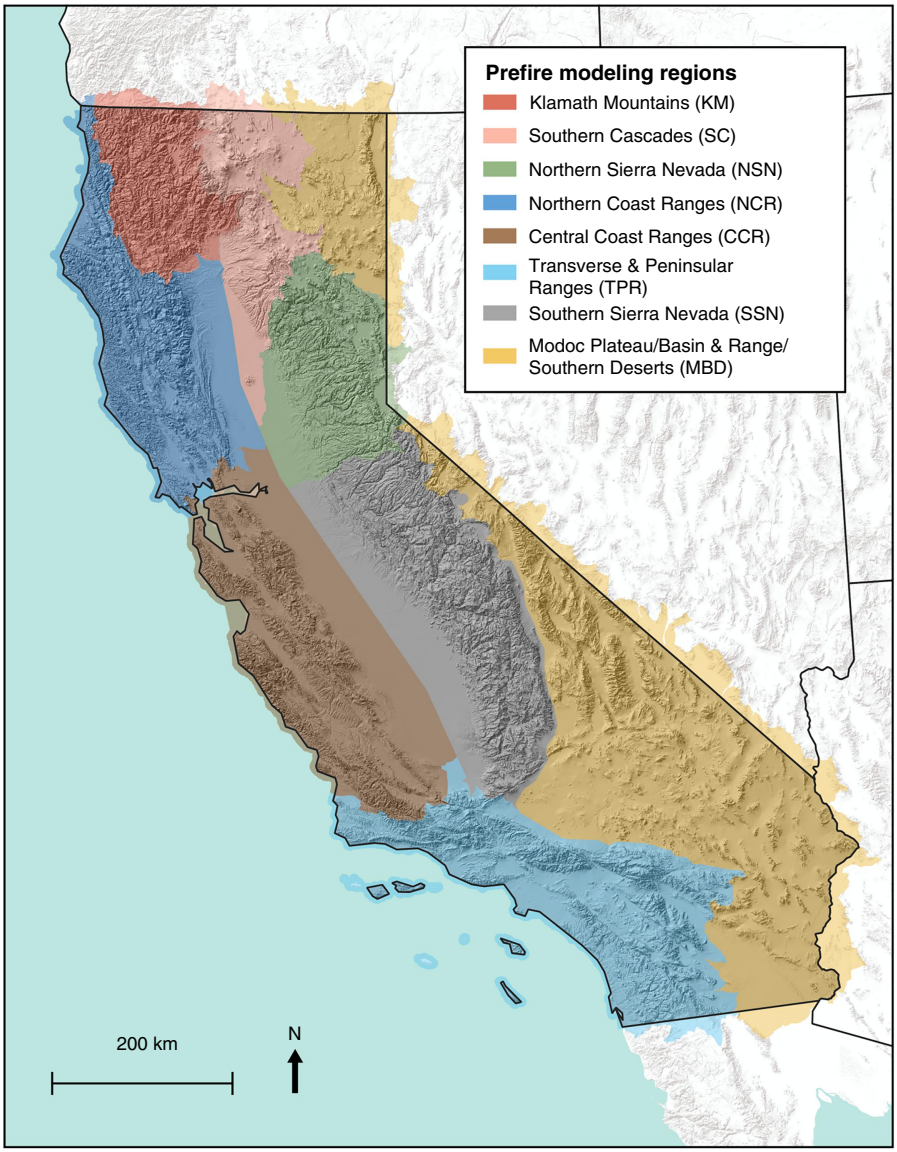

Fig. 1. Prefire modeling regions across California; outer region boundaries were adjusted to match the HU10 watershed boundaries and were split across the centerlines of large valleys.

between the fire and the first triggering rainstorm (Kean *et al.* 2019). Knowing the potential of postfire hazards under hypothetical burn scenarios can provide emergency managers, road and facility engineers, and flood control officers with information to better prepare for inevitable wildfires.

More advanced knowledge of wildfire effects and associated impacts across California is required to make informed decisions prior to fire and build additional resilience against postfire hazards under a changing climate (Kean and Staley 2021). To contribute to this effort, we developed a statewide map that predicts the spatial distribution of fire severity and runoff-generated postfire debris-flow hazards. Benefits of this statewide modeling and mapping effort include (1) an assessment of threats to downstream values at risk (e.g. homes, bridges, and other infrastructure) that can be used to prioritize fuels treatments, (2) readily available data and maps that can immediately inform active suppression operations and emergency response efforts, (3) information that local governments can apply in residential development plans, zoning maps, and local hazard mitigation plans, (4) data to identify additional resource needs and support funding opportunities from federal and state sources (e.g. grant funds), and (5) information to assist in identifying and designing potential mitigation measures to reduce downstream hazards.

Methods

Prefire modeling regions

Because fire behavior and severity vary across California (e.g. Parsons *et al.* 2010; Estes *et al.* 2017), we determined prefire modeling regions based upon patterns in fuels, topography, and climate. To account for differences in fuel

type, we referred to the National Vegetation Classification Standard zones (US Forest Service 2009), which group existing vegetation types that co-occur within landscapes with similar climate, substrates, and ecological processes. To account for differences in topography, and other physiographic controls, we referred to a map of geomorphic provinces that are characterized by distinct geology, topography, and plant communities (California Geological Survey 1997). Once the initial regions were identified, their margins were further refined using the watershed hydrologic unit (HU10) boundaries within the Watershed Boundary Dataset (US Geological Survey 2024) and valley centerlines (Fig. 1).

Simulation of regional fire and burn severity for predicting postfire debris-flow hazards across California

As numerous factors affect fire behavior (e.g. van Mantgem *et al.* 2013; Zald and Dunn 2018), many of which cannot be estimated prior to fire, we simulated fire severity across each prefire modeling region using established relationships between observed existing vegetation type and the change in surface and subsurface organic matter composition (i.e. differenced Normalized Burn Ratio: dNBR; Staley *et al.* 2018; Kean and Staley 2021). Staley *et al.* (2018) developed a two-parameter Weibull cumulative distribution function (CDF) for 282 unique LandFire Existing Vegetation Type (EVT) classes present within 3163 historical burn areas across the western US using data available between 2001 and 2014 (LandFire 2022). To incorporate change in landcover across the state associated with disturbances since 2014, including wildfire, we created a map of the most recent EVT classes with established CDF parameters (Staley 2018). Where there were no data values or EVT classes present without corresponding CDF parameters, we back sampled from previous EVT datasets to assign EVT classes that closely matched observed conditions. This enabled us to create a continuous, statewide map of EVT data for which corresponding CDF parameters exist.

To simulate dNBR, we used the CDF parameters for each EVT class and the same parameters for each prefire region. The cumulative probability of the Weibull CDF at which fire severity is being simulated is represented by P_{dsim}. For example, entering the CDF at a P_{dsim} of 0.5 (50th percentile) describes the median fire severity for each EVT class; entering at a P_{dsim} of 0.9 (90th percentile) describes an abnormally high fire severity for that EVT class. We chose to calibrate the P_{dsim} parameter for each prefire region and two calibration approaches are described in the following section. These approaches do not capture variability due to local conditions (e.g. wind direction) but aim to represent potential regional outcomes based on historical burn severity observations. Simulated dNBR for each EVT class was estimated from Eqn 1 in Table 1. Lastly, the simulated dNBR map was classified into Burned Area Reflectance Classification (BARC) categories of unburned/very low, low, moderate, and high burn severity, as described in the next section.

To predict the debris-flow hazard within the first year following fire, the simulated dNBR and BARC maps, along with a fixed 15-min rainfall intensity (I_{15}) of 24 mm h^{-1}, were used as input variables in the US Geological Survey's (USGS) postfire debris-flow hazard assessment model equations for predicting debris-flow likelihood, volumes of sediment deposited by debris flows (herein referred to as 'volume'), and rainfall intensity-duration thresholds (Table 1). We used an I_{15} of 24 mm h^{-1}, as I_{15} is a better predictor of runoff-generated postfire debris-flow occurrence than rainfall intensities measured over longer durations (e.g. Kean *et al.* 2011; Staley *et al.* 2013; Thomas *et al.* 2023) and is also the rainfall intensity metric used in the volume model (Gartner *et al.* 2014). Furthermore, 24 mm h^{-1} is close to the mean and median I_{15} associated with a 1-year recurrence interval within our modeled area. Staley *et al.* (2020) show that postfire debris flows are most commonly triggered by the 1-year recurrence interval I_{15}. For this reason, the 24 mm h^{-1} rainfall intensity is frequently applied in USGS postfire debris-flow hazard assessments (e.g. Staley *et al.* 2017; Barnhart *et al.* 2021). We used a debris-flow likelihood value of 50% to solve for rainfall intensity-duration thresholds (Table 1).

Calibration methods

We considered two calibration methods, one focused on reproducing BARC maps (herein referred to as the 'BARC map calibration') whereas the other focused on reproducing the best match to the debris-flow likelihood results produced by the USGS debris-flow likelihood model using observed dNBR values (herein referred to as the 'DFL calibration'). We refer to the USGS debris-flow likelihood model results as 'observed' because the values are calculated from observed dNBR and observed BARC values from postfire satellite data. Each method used a fire calibration set composed of California wildfires in the Monitoring Trends in Burn Severity (MTBS) database for 2020 and 2021 that contain low-moderate BARC breaks and fire area above 10 km^2 (MTBS 2022; Fig. 2). We focused on low-moderate BARC breaks instead of moderate-high BARC breaks because the USGS debris-flow likelihood and volume models do not distinguish between moderate and high BARC values. We limited our calibration of P_{dsim} to these fires for several reasons, including (1) the distribution of fires included in the calibration set are spatially distributed across a wide range of physiographic regions; (2) the difference in mean MTBS burn severity in the calibration set is not statistically significant ($P = 0.26$) compared to the full set of fires in the MTBS dataset from 1984 to 2021; and (3) the unavailability of post-2021 MTBS data at the time of analysis. We calculated the median of the low-moderate BARC break values for the calibration fires for each prefire modeling region (Fig. 2) to generate regional BARC break values that were used to

Table 1. Summary of prefire simulated dNBR equation and USGS postfire debris-flow hazard models.

Name	Equation	Citation
Simulated differenced Normalized Burn Ratio (dNBR) for each Existing Vegetation Type (EVT) class (SimdNBR)	$\text{SimdNBR} = \lambda[-\ln(1 - P_{dsim})]^{1/\kappa} \times 2000 - 1000$ (1) λ = best-fit scale parameter for each Weibull cumulative distribution function (CDF) κ = best-fit shape parameter for each Weibull CDF P_{dsim} = percentile of the Weibull CDF at which fire severity is being simulated	Staley *et al.* (2018)
Debris-flow likelihood (DFL)	$\text{DFL} = \exp(X)/(1 + \exp(X))$ (2) $X = -3.63 + (0.41 \times X_1 \times R) + (0.67 \times X_2 \times R) + (0.7 \times X_3 \times R)$ X_1 = proportion of upslope basin area burned at high or moderate severity with gradient in excess of 23 degrees X_2 = average dNBR of upslope basin area divided by 1000 X_3 = soil erodibility index of the fine fraction of soils (i.e. Kf factor) R = 15-min rainfall accumulation (mm)	Staley *et al.* (2016)
Debris-flow volume (DFV, m^3)	$\text{DFV} = \exp(4.22 + 0.39 \times \text{sqrt}(I_{15}) + 0.36 \times \ln(\text{Bmh}) + 0.13 \times \text{sqrt}(\text{Relief}))$ (3) I_{15} = 15-min rainfall intensity (mm h^{-1}) Bmh = upslope basin area burned at high or moderate severity (km^2) Relief = upslope basin relief (m)	Gartner *et al.* (2014)
Rainfall intensity-duration threshold (T, mm h^{-1})	$T = (\ln(\text{DFL}/1 - \text{DFL}) + 3.63)/((0.41 \times X_1) + (0.67 \times X_2) + (0.7 \times X_3))$ (4) DFL = likelihood value used for debris-flow threshold (i.e. DFL = 0.5) X_1 = proportion of upslope basin area burned at high or moderate severity with gradient in excess of 23 degrees X_2 = average dNBR of upslope area divided by 1000 X_3 = soil erodibility index of the fine fraction of soils (i.e. Kf factor)	Staley *et al.* (2017)

calculate the area burned at moderate and high severity. A calibrated P_{dsim} value was determined for each fire. The regional P_{dsim} value was calculated as the median of the P_{dsim} values for fires in the same region.

For the BARC map calibration, P_{dsim} was chosen to produce a combined moderate and high BARC area, produced from modeled dNBR values and regional BARC breaks, that is equal to or greater than the observed combined moderate and high BARC area. For the DFL calibration, P_{dsim} was calibrated to produce the lowest Root Mean Square Error (RMSE) for the simulated debris-flow likelihood and the observed debris-flow likelihood results. We use the observed MTBS dNBR values, fire-specific MTBS BARC breaks, and 15-min rainfall intensity of 24 mm h^{-1} for basins inside the fire perimeter as input to the USGS debris-flow likelihood model to calculate observed debris-flow likelihood results. These results were generated using the postfire debris-flow ('pfdf') Python library (King 2023). The DFL calibration procedure is summarized in a flowchart in Fig. 3. For the DFL calibration, basins with less than 75% of their area inside the fire perimeter or a median observed dNBR value below the fire-specific MTBS unburned-low BARC break were excluded from the calibration.

Calibration assessment

To assess which calibration approach produced better results, we compared the Nash-Sutcliffe Efficiency (NSE) for the two calibration approaches. NSE was calculated as:

$$1 - \frac{\sum_{i=1}^{n}(\text{DFL}_{obs}^{i} - \text{DFL}_{sim}^{i})^2}{\sum_{i=1}^{n}(\text{DFL}_{obs}^{i} - \overline{DFL}_{obs})^2} \quad (5)$$

where DFL_{obs} is the fire-wide mean observed debris-flow likelihood calculated from the USGS debris-flow likelihood model (Staley *et al.* 2016), DFL_{sim} is the fire-wide mean simulated debris-flow likelihood for the respective calibration approach, i represents each calibration fire, and n is the total number of calibration fires. Regional BARC breaks and regional P_{dsim} values were used for the simulated debris-flow likelihood model runs whereas observed MTBS BARC breaks were used for the observed debris-flow likelihood

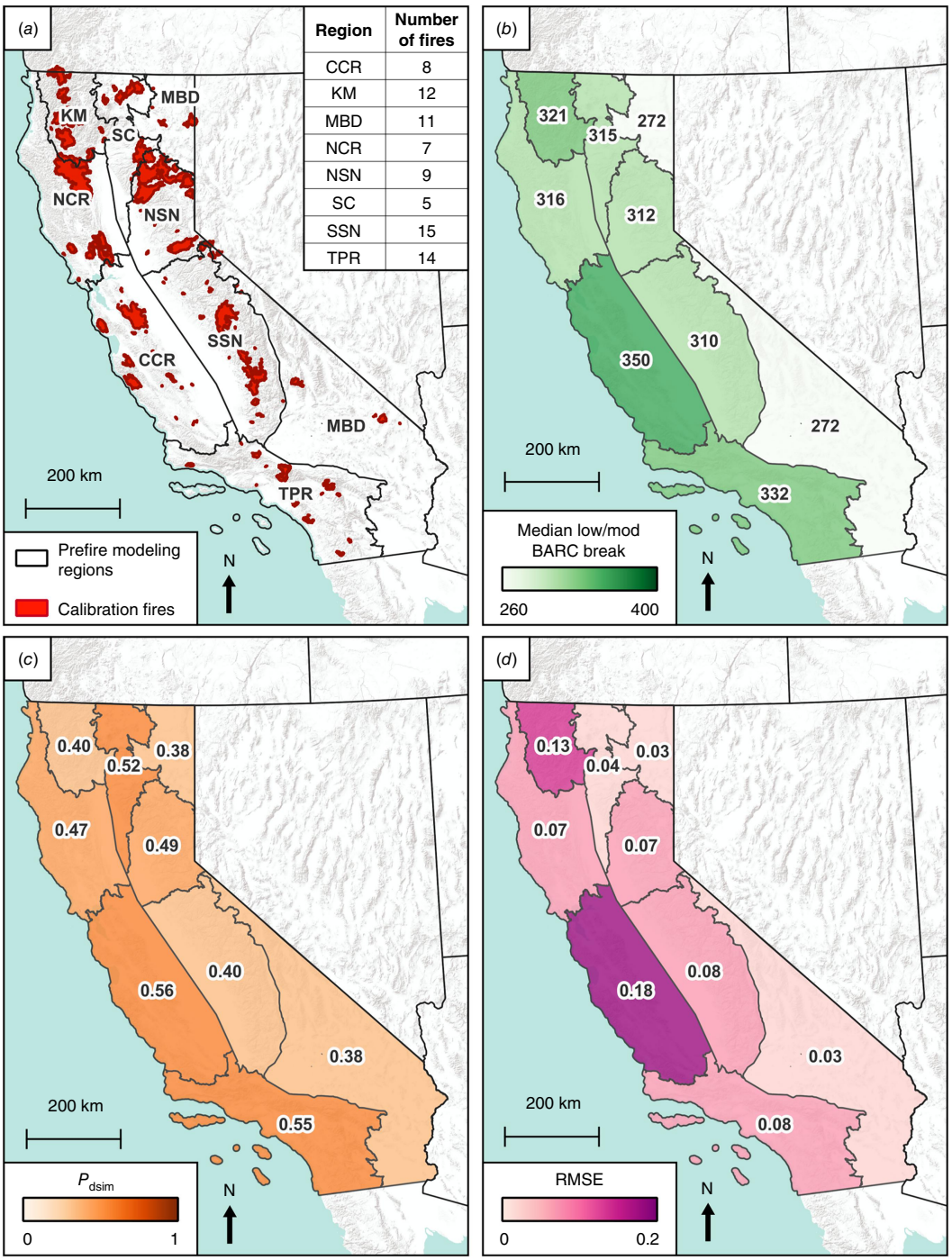

Fig. 2. P_{dsim} calibration methods. Calibration fires (n = 81) from 2020 to 2021, with table showing number of fires by region (*a*); median low-moderate Burned Area Reflectance Classification (BARC) break values (*b*); regional P_{dsim} values (*c*); Root Mean Square Error (RMSE) calculated to compare the simulated and observed debris-flow likelihood for basins inside the fire perimeters (*d*). Abbreviations: CCR, Central Coast Ranges; KM, Klamath Mountains; MBD, Modoc Plateau, Basin and Range, and Southern Deserts; NCR, Northern Coast Ranges; NSN, Northern Sierra Nevada; SC, Southern Cascades; SSN, Southern Sierra Nevada; TPR, Transverse and Peninsular Ranges.

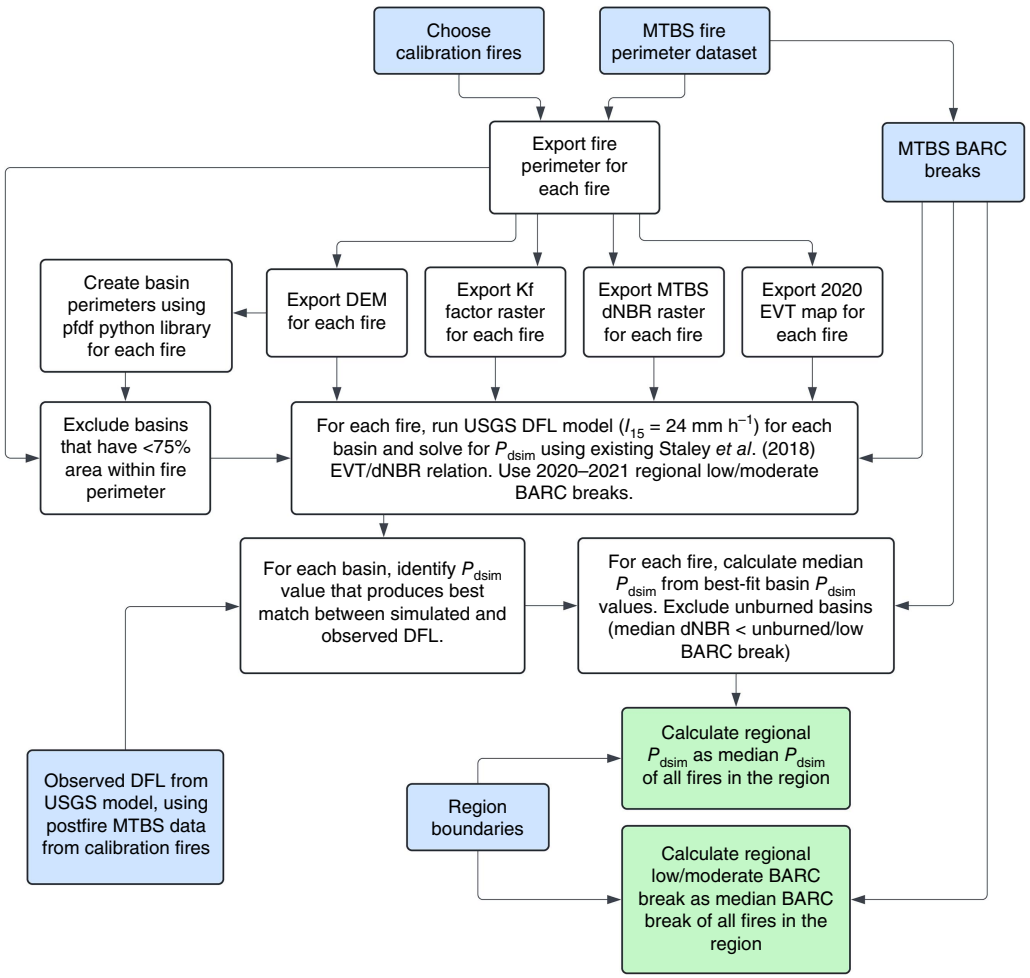

Fig. 3. Flowchart summarizing the regional P_{dsim} calibration and low-moderate Burned Area Reflectance Classification (BARC) break calculation procedure detailed in the Methods section. Inputs, outputs and intermediate steps are shown in blue, green, and white boxes, respectively. Abbreviations: DFL, debris-flow likelihood; dNBR, differenced Normalized Burn Ratio; DEM, Digital Elevation Model; EVT, Existing Vegetation Type; MTBS, Monitoring Trends in Burn Severity.

model runs. We focused our discussion on the calibration approach that produced the highest NSE.

Postfire debris-flow model and prefire inputs

The simulated dNBR map was generated from the EVT map (Table 2) using the established EVT-dNBR relationships (Staley *et al.* 2018) and the regional P_{dsim} values. The simulated dNBR map was then classified into a simulated BARC map using the regional median low-moderate BARC break values.

To only model debris-flow likelihood and volume where runoff-generated postfire debris flows could initiate, we adopted the standard USGS basin area criteria (0.025–8 km^2; Staley *et al.* 2016) and masked the model domain to prevent basin delineation in flat areas (Table 2). Though flat areas could experience inundation from debris flows generated upstream, the USGS models used in this study are only intended to model initiation, not runout. We then ran the debris-flow likelihood and volume models within the pfdf Python library (King 2023) separately for each subbasin hydrologic unit (HU8) boundary in California in the Watershed Boundary Dataset to increase computational efficiency relative to modeling the full state in one iteration. We used subbasins (HU8) for most regions and watersheds (HU10) in the Basin and Range and Southern Deserts region, which we found to minimize basin delineation artifacts.

Annual probability of postfire debris flows across California

The annual probability of occurrence of a particular rainfall intensity varies widely across the diverse climates of California. Therefore, climatological information was required to predict the annual exceedance probability $P(R > T)$ of a rainfall intensity (R) exceeding the modeled rainfall intensity

Table 2. Datasets used in the statewide prefire modeling of postfire debris-flow hazards.

Dataset name	Description	Source
Cumulative distribution function (CDF) parameters	Best-fit Weibull CDF parameters that relate each Existing Vegetation Type (EVT) class to a differenced Normalized Burn Ratio (dNBR) value; used to calculate simulated dNBR.	Staley (2018)
EVT[A,B]	EVT rasters (30-m) used to generate simulated dNBR inputs.	LandFire (2022)
Calibrated P_{dsim} and Burned Area Reflectance Classification (BARC) break values by region	Calibrated P_{dsim} values and the median low-moderate BARC breaks (calibration fire dataset) for each of the eight prefire modeling regions.	MTBS (2022)
Digital Elevation Model (DEM)[A]	Mosaic of 1/3 arc-second digital elevation tiles.	US Geological Survey (2024)
Kf factor[A]	Soil erodibility index of the fine fraction of soils; STATSGO soil polygons assigned with 'KFFACT' attribute; values less than 0 were excluded from the analysis.	Schwartz and Alexander (1995)
Model domains[A]	Subbasin (HU8) and watershed (HU10) boundary polygons from the Watershed Boundary Dataset that were used to define the model domain.	US Geological Survey (2023)
Masks[A]	A set of masks were used to exclude areas of low slope or open water from the model domain where debris flows are unlikely to initiate and to minimize artifacts in basin delineation. Valley mask: A focal statistics algorithm was used to calculate the standard deviation of elevation within a 200 m radius of every cell in the DEM. Clusters of cells with values less than or equal to 5 m were converted to polygons, and all polygons with an area less than 1 km^2 were deleted. Sink mask: To create the sink mask, the portion of the pfdf Python library (King 2023) which generates a flow direction raster was run and DEM conditioning criteria of filled pits, filled depressions, and unresolved flats was selected. The areas marked as null in this output directly correspond to areas mapped erroneously as basins. We converted these clusters of null values to polygons and deleted all polygons with an area less than 1 km^2. To ensure that all polygons of the sink mask were in valley areas, we deleted all polygons that did not intersect the valley mask. Water mask: Two data sources were used to mask out large bodies of water, including water bodies boundaries and the 2022 EVT open water classification.	LandFire (2022), US Geological Survey (2020, 2023)

[A]Projected to California Teale Albers (datum: NAD 1983); 10-m resolution.
[B]We used the LandFire EVT rasters to generate two EVT maps that contain the most recent EVT classes with established CDF parameters to use in the calibration of P_{dsim} (2020 EVT map) and the prefire modeling (2022 EVT map). Pixels that contained a no data value in the EVT maps were assigned an EVT code of 7294 (i.e. barren).

threshold (T). The National Oceanic and Atmospheric Administration (NOAA) Atlas14 product (Perica *et al.* 2014) describes the 15-min rainfall intensity associated with particular recurrence intervals (RI) from 1 to 1000 years. These products are spatially continuous across the state with a cell size of 800 m. The relationship between a particular rainfall intensity and its expected RI is log-linear and can be expressed as Eqn 6 in Table 3. To estimate m and b, the mean values of the 1- and 50-year rainfall intensity (Fig. 4) at each basin were extracted using a zonal statistics algorithm, and m and b were estimated using Eqns 7 and 8 in Table 3. The RI of the modeled rainfall intensity threshold was then computed for each basin. To convert RI to annual exceedance probability P, we used Eqn 9 in Table 3.

With this workflow, we estimated the RI and associated annual exceedance probability of the modeled rainfall intensity threshold at each basin, after it has burned. However, as the aim of this study is to model debris-flow likelihood before a fire occurs, a true prefire estimate of postfire debris-flow likelihood should also take into account the probability that a fire actually occurs (i.e. $P(F)$) in a particular basin (e.g. Kean and Staley 2021). For typical climatic conditions (i.e. neither drought nor extremely wet conditions), we expect a weak relationship between the occurrence of threshold-exceeding rainfall intensity and fire, and we treat their occurrence as independent of one another. For typical conditions, which we aim to model in this study, we estimate the annual probability of a postfire debris flow is thus the product $P(F) \times P(R > T)$.

To estimate $P(F)$ we used the wildfire simulation model (FSim) product developed by Pyrologix in conjunction with the US Forest Service and California Department of Forestry and Fire Protection, which estimates annual fire probability (regardless of severity) in a spatially continuous 30-m grid across the state (Vogler *et al.* 2021; US Forest Service 2023; Fig. 4). The FSim product captures variability in localized

Table 3. Summary of equations used to calculate annual probability.

Name	Equation	Citation
Recurrence interval (RI)	$RI = 10^{m I_{15} + b}$ (6) I_{15} = 15-min rainfall intensity (mm h^{-1}) m = slope of the log-linear relationship between intensity and RI (Eqn 7) b = y-intercept of the log-linear relationship between intensity and RI (Eqn 8)	Perica *et al.* (2014)
m, b	$m = \frac{\log(50) - \log(1)}{50yrI_{15} - 1yrI_{15}}$ (7) $b = -m \times 1yrI_{15}$ (8) $1yrI_{15}$ = 1-year rainfall intensity (mm h^{-1}) $50yrI_{15}$ = 50-year rainfall intensity (mm h^{-1})	Perica *et al.* (2014); m and b calculated using zonal statistics algorithm in QGIS (version 3.34.1)
Annual exceedance probability (P)	$P = 1 - e^{-1/RI}$ (9) RI = recurrence interval (Eqn 6)	Feller (1991)

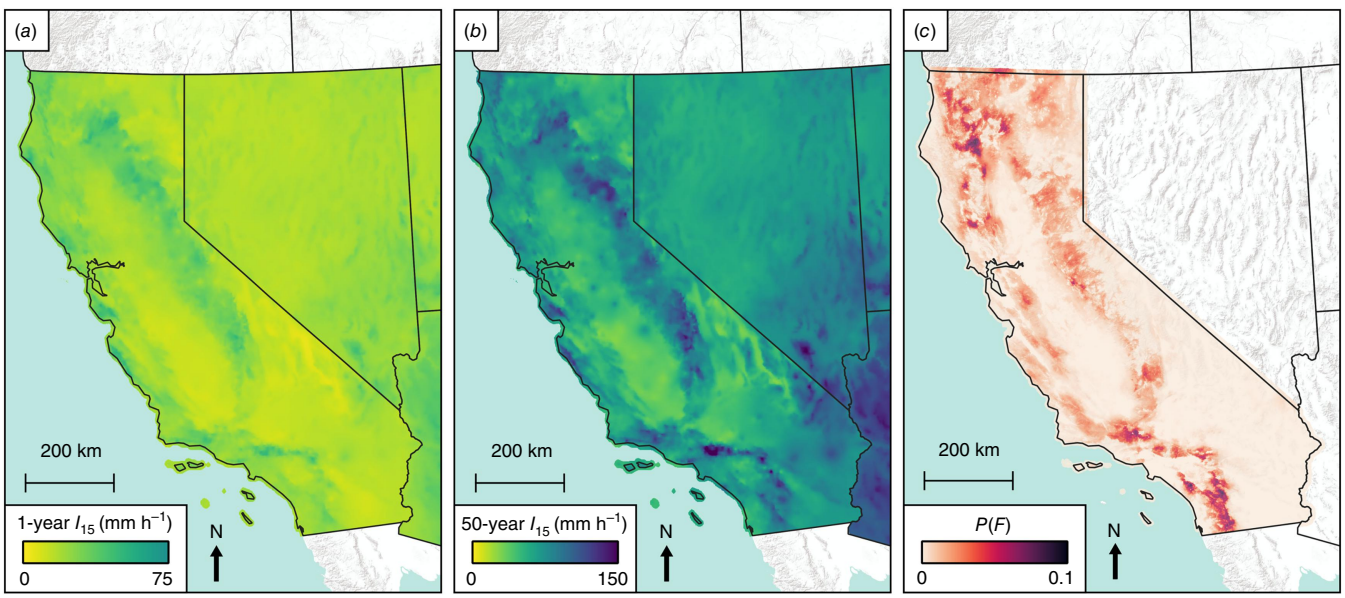

Fig. 4. Maps of inputs to the annual probability analysis: Atlas14 1-year (*a*) and 50-year (*b*) 15-min rainfall intensity (I_{15}), and the FSim annual burn probability product (*P(F)*) (*c*; Vogler *et al.* 2021; US Forest Service 2023).

fire conditions and behavior, including changes in fuel moisture content, combinations of wind speed, wind direction, topography, and historical fire occurrence across the landscape (Vogler *et al.* 2021; U.S. Forest Service 2023). We then computed the mean $P(F)$ value for each basin and multiplied it by the basin's $P(R > T)$ prediction to yield an annual probability of fire followed by above-threshold rainfall in the year following fire. The prefire modeling and annual probability procedure is summarized in Fig. 5.

Results

Existing vegetation type map

The Existing Vegetation Type (EVT) classes that we replaced within the EVT maps varied in total area by region. Approximately 20% of the prefire modeling region domain was mapped with EVT classes drawn from preceding EVT rasters used in both the calibration of P_{dsim} (2020 EVT map) and the simulated differenced Normalized Burn Ratio (dNBR)

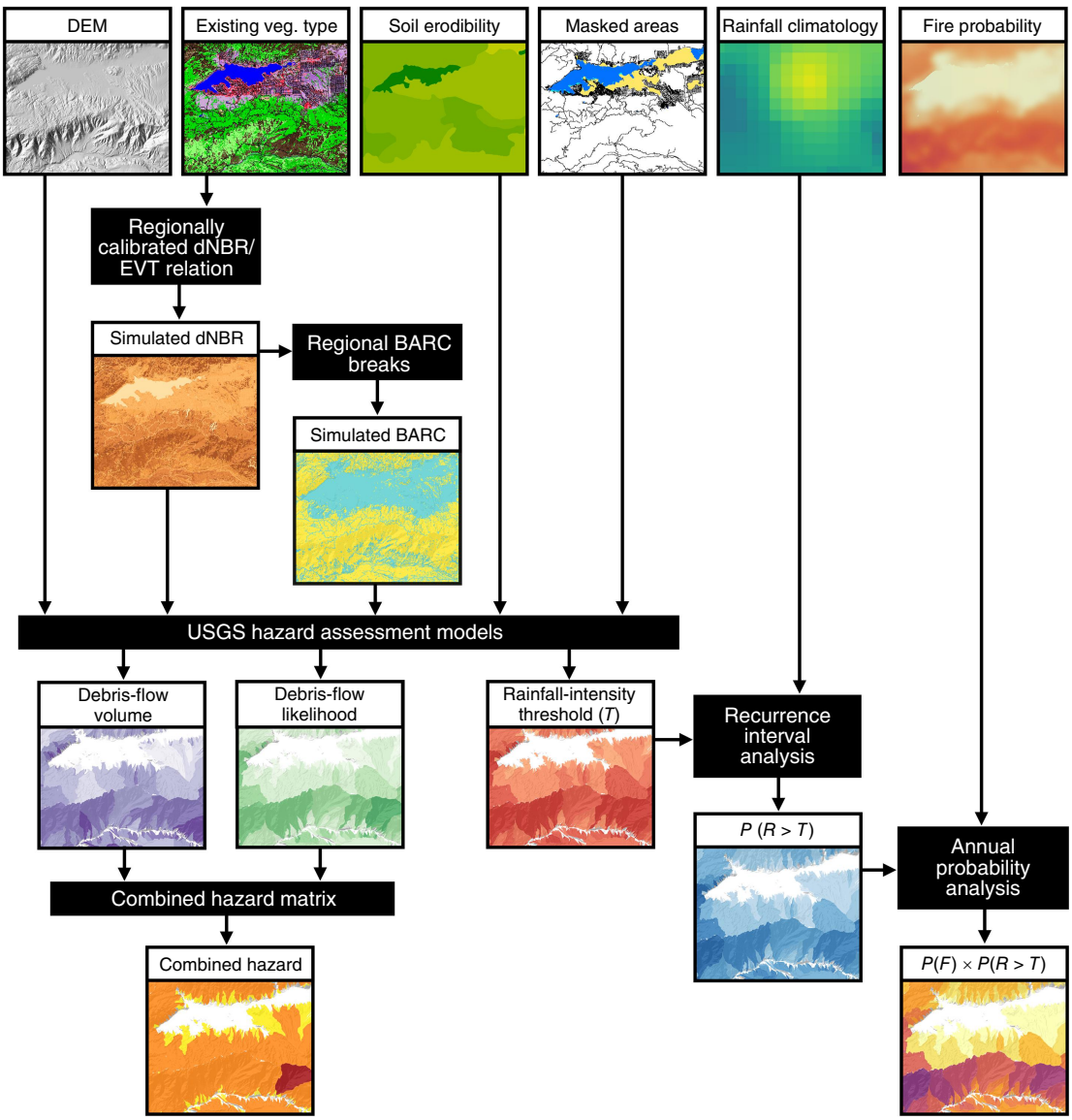

Fig. 5. Flowchart outlining the prefire hazard modeling procedure and associated map products. We used a 15-min rainfall intensity of 24 mm h^{-1} as an input to the debris-flow likelihood and volume models. This procedure is detailed in the Methods section. Abbreviations: BARC, Burned Area Reflectance Classification; dNBR, differenced Normalized Burn Ratio; EVT, Existing Vegetation Type; RMSE, Root Mean Square Error; *R*, rainfall intensity; *T*, modeled rainfall intensity threshold; *P*(*R* > *T*), annual probability that the 15-min triggering rainfall intensity is exceeded for a debris-flow likelihood value of 50%; *P*(*F*), annual fire probability; *P*(*F*) × *P*(*R* > *T*), annual probability of a fire and subsequent above-threshold rainfall intensity within the year following fire.

maps used in the prefire modeling (2022 EVT map; Fig. 6). The total replaced area of EVT classes ranged from ~5% in the Klamath Mountains to ~35% in the Central Coast Ranges and Southern Sierra Nevada and mostly consisted of low-elevation slopes along the margin of the Sacramento and San Joaquin Valleys.

Comparison of calibration methods

We compared results for two P_{dsim} calibration methods to results for P_{dsim} of 0.50 (Fig. 7) for 81 calibration fires (Table 4). The DFL calibration produced a higher Nash-Sutcliffe Efficiency value (NSE = 0.57) relative to the Burned Area Reflectance Classification (BARC) map calibration (NSE = 0.37) with regionally calibrated P_{dsim} values or using a fixed P_{dsim} of 0.50 (NSE = 0.22; Fig. 7). Because the DFL calibration produced the highest NSE value of the two calibration methods that we considered, we focused our results and discussion on the results from the DFL calibration. We also considered the consequences of predicting debris-flow likelihood using a fire-specific P_{dsim} instead of the regional median P_{dsim}. The fire-specific P_{dsim}

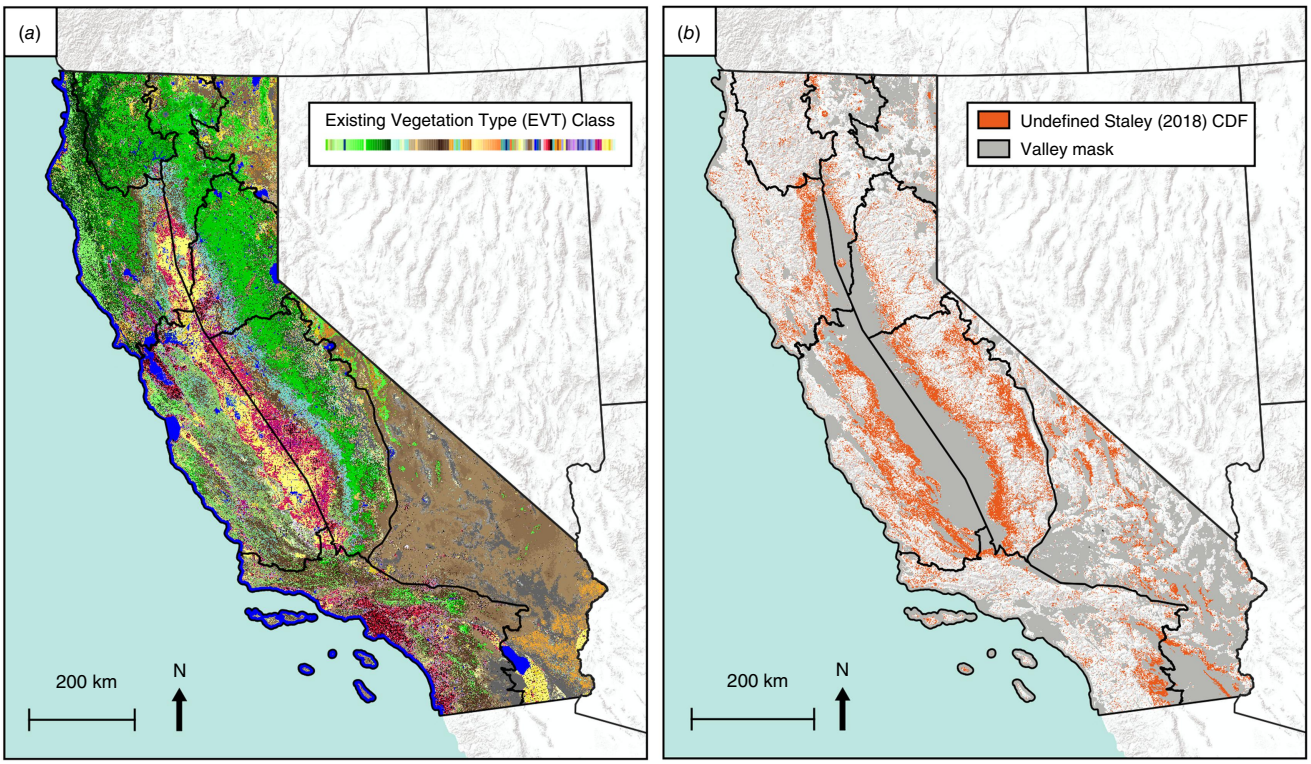

Fig. 6. 2022 EVT map (Table 2) showing the spatial distribution of Landfire EVT classes across the prefire modeling regions, with each Landfire EVT class shown in a different color (*a*) and location of replaced EVT classes across the California prefire modeling region domain, where a Staley (2018) CDF is undefined (*b*).

produced a better relationship between the simulated and observed debris-flow likelihood (NSE = 0.98; Fig. 7).

The Root Mean Square Error (RMSE) values of the calibration were generally low but varied by region (Fig. 7, Table 5). For example, calibration fires for the Central Coast Ranges produced the highest RMSE (0.18) while the region that includes the Modoc Plateau, Basin and Range, and Southern Deserts produced the lowest RMSE (0.03) (Fig. 7, Table 5). Figs 2 and 8 present P_{dsim} results for each region. Basins where the simulated dNBR closely matched the observed dNBR typically produced the closest match between simulated and observed debris-flow likelihood (Fig. 9). Observed basin dNBR exhibits a much wider range in values relative to simulated P_{dsim} values (Fig. 9). The limited range of simulated dNBR values constrained the ability of the model to reproduce observed dNBR distributions. Regions with lower moderate BARC breaks typically produced lower calibrated P_{dsim} values (Fig. 8).

The wide range in calibrated P_{dsim} values (Figs 2, 8) is strong evidence that fire behavior and severity vary widely even for a single region. For some regions, we reproduced the mean debris-flow likelihood using a regional calibration. In particular, the Modoc Plateau, Basin and Range, Southern Deserts and the Southern Cascades produced relatively low RMSE values (0.03 and 0.04, respectively) while the Klamath Mountains (RMSE = 0.13) and Central Coast Ranges (RMSE = 0.18) produced the highest RMSE. The Northern Coast Ranges (RMSE = 0.07), Northern Sierra Nevada (RMSE = 0.07), Southern Sierra Nevada (RMSE = 0.08) and Transverse and Peninsular Ranges (RMSE = 0.08) produced results with intermediate RMSE. In most cases, the ability to predict the mean debris-flow likelihood is much better than the ability to predict the debris-flow likelihood of basins within an individual fire perimeter (Table 5). For example, the RMSE for the fire-wide mean debris-flow likelihood is substantially lower than the RMSE calculated from all calibration basins in the region (RMSE = 0.02 for the fire mean versus RMSE = 0.21 for calibration basins for the fire-specific P_{dsim} and RMSE = 0.09 for the fire mean versus RMSE = 0.22 for calibration basins for the regional P_{dsim}; Table 5).

Statewide prefire map products

Using the methods described above, we generated nine map products relevant to predicting postfire debris-flow hazard prior to fire (Rossi *et al.* 2025). The simulated dNBR and simulated BARC (four classes; Fig. 10) maps were generated prior to running the USGS models and resulted from the simulated burning of existing vegetation according to the regional

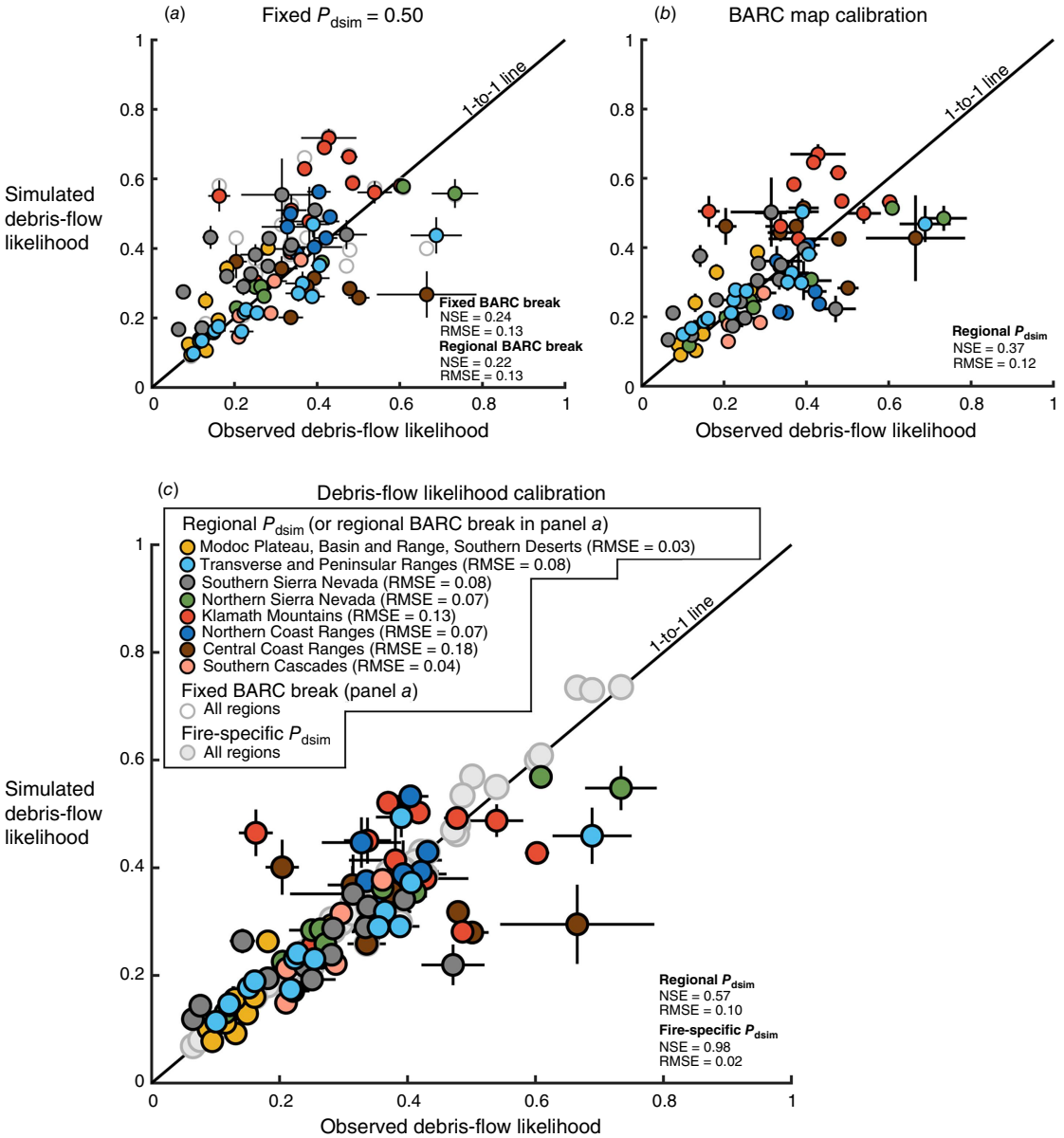

Fig. 7. Comparison of fire-wide mean debris-flow likelihood for fixed P_{dsim} = 0.50 (*a*) and calibration to best match to percent moderate-high burn severity (i.e. Burned Area Reflectance Classification (BARC) map calibration) (*b*), and lowest Root Mean Square Error (RMSE) for observed and simulated debris-flow likelihood (i.e. DFL calibration) (*c*). Uncertainty bars show two standard errors of the mean for the basins inside the respective fire perimeter. The uncertainty bars indicate the relative width of the distributions for the simulated and observed debris-flow likelihood for a single fire (since the sample size for simulated and observed debris-flow likelihood match for the same fire). Results and statistics are for simulated and observed debris-flow likelihood for basin $dNBR_{obs}$ > unburned-low BARC break (T_{low}). Abbreviations: dNBR, differenced Normalized Burn Ratio; NSE, Nash-Sutcliffe Efficiency.

P_{dsim} and regional BARC breaks that provided the best match of simulated to observed debris-flow likelihood results. The spatial data generated by the USGS models include debris-flow likelihood (calculated using I_{15} = 24 mm h^{-1}), rainfall intensity threshold (calculated using debris-flow likelihood = 50%), volume, and combined hazard classification (Fig. 10). Combined hazard classification was determined by combining the USGS modeled debris-flow likelihood and volume and assigning a combined hazard class as low, moderate, or high (Cannon *et al.* 2010). The products associated with the annual probability methods include annual probability of exceedance of the predicted rainfall intensity threshold, annual fire probability, and annual probability of fire and subsequent above-threshold rainfall in the year following fire (Fig. 10).

Table 4. List of calibration fires by region.

Region	Calibration fires[A]
Central Coast Ranges	Carmel (30 km^2), Crews (23 km^2), CZU August Lightning (348 km^2), Dolan (503 km^2), Mineral (121 km^2), River (209 km^2), SCU Lightning Complex (1642 km^2), Willow (13 km^2)
Klamath Mountains	Cronan (31 km^2), Devil (37 km^2), Fawn (37 km^2), Haypress (828 km^2), Knob (10 km^2), McCash (388 km^2), **McFarland** (492 km^2), Monument (915 km^2), Red Salmon Complex (597 km^2), Salt (51 km^2), Slater (639 km^2), Zogg (230 km^2)
Modoc Plateau/Basin and Range/Southern Deserts	Baccarat (41 km^2), Coles Flat (167 km^2), **Dexter** (12 km^2), Gold (88 km^2), Junction Ranch (38 km^2), Mountain View (58 km^2), **North** (28 km^2), **Sheep** (118 km^2), **Slink** (107 km^2), **Tamarack** (284 km^2), W-5 Cold Springs (340 km^2)
Northern Coast Ranges	August Complex (4325 km^2), Glass (275 km^2), Hennessey (1272 km^2), **McFarland** (492 km^2), Meyers (10 km^2), Wallbridge (223 km^2), Woodward (20 km^2)
Northern Sierra Nevada	Caldor (917 km^2), **Dixie** (3965 km^2), Hog (39 km^2), Loyalton (184 km^2), **North** (28 km^2), North Complex (1281 km^2), River (11 km^2), **Sheep** (118 km^2), Sugar (439 km^2)
Southern Cascades	Antelope (574 km^2), Caldwell (331 km^2), **Dixie** (3965 km^2), Lava (106 km^2), Tennant (48 km^2)
Southern Sierra Nevada	Bluejay (28 km^2), Castle (706 km^2), Creek (1544 km^2), **Dexter** (12 km^2), French (111 km^2), KNP Complex (364 km^2), Moc (13 km^2), Rattlesnake (37 km^2), River (41 km^2), **Slink** (107 km^2), Stagecoach (31 km^2), **Tamarack** (284 km^2), Tiltill (11 km^2), Walkers (36 km^2), Windy (396 km^2)
Transverse and Peninsular Ranges	Alisal (72 km^2), Apple (131 km^2), Blue Ridge (56 km^2), Bobcat (468 km^2), Bond (27 km^2), Creek 5 (18 km^2), El Dorado (90 km^2), India (98 km^2), Lake (125 km^2), Ranch 2 (18 km^2), Silverado (51 km^2), Snow (26 km^2), Southern (22 km^2), Valley (67 km^2)

[A]Fire area included in parentheses; fires that were used in more than one region are listed in bold text.

Discussion

Limitations of simulating dNBR

One limitation of our approach is that we used relationships between Existing Vegetation Type (EVT) and differenced Normalized Burn Ratio (dNBR) developed by Staley *et al.* (2018) and new EVT classes have been introduced in California since the Staley *et al.* (2018) study. Instead of developing new EVT-dNBR relationships for the new EVT classes, we reclassified the new EVT classes with previous EVT classes. Updated cumulative distribution function (CDF) parameters could be calculated for areas where we applied replacement EVT classes, but it remains unclear how much these new EVT classes might impact simulated fire severity. For example, California Ruderal Grassland, a new grassland EVT class that widely occurs within the Central Coast Ranges and Southern Sierra Nevada, was replaced in our EVT map with a more spatially variable set of preceding EVT classes that included grassland, shrubland, and forest EVT classes. Updated CDF parameters for this new grassland EVT are likely to represent similar fire severity to our replacement grassland EVT class. In this example, our replacement EVT classes of shrubland and forest likely simulate higher fire severity than the new grassland EVT class and thus we provide a more conservative representation of fire severity in these locations.

P_{dsim} calibration

Expanding the calibration dataset to include additional fires may influence the regionally calibrated P_{dsim} values, but our ability to reproduce variance in basin debris-flow likelihood is unlikely to improve by expanding the calibration dataset. This is because our current approach for predicting dNBR produced a relatively limited range in dNBR values relative to real fire behavior (Fig. 9) and because predicting variability in fire behavior is difficult even with more sophisticated approaches that predict burn severity (Wells *et al.* 2023).

The model requires calibration of a single parameter (P_{dsim}), and we calibrated the model to produce a close match between the mean simulated and observed debris-flow likelihood. Increasing P_{dsim} will shift the mean debris-flow likelihood higher while decreasing P_{dsim} will shift the mean debris-flow likelihood lower. Even within a single region, there was a wide range in fire intensity, which required different values of P_{dsim} to match mean fire-wide debris-flow likelihood (Fig. 8). Because fire-specific P_{dsim} values varied for a region (Fig. 8), we used the median P_{dsim} for a region to estimate debris-flow likelihood and produce our debris-flow likelihood maps. The relatively minimal improvement in Root Mean Square Error (RMSE) for basins using a fire-specific P_{dsim} relative to a regional P_{dsim} (RMSE = 0.21 for fire-specific P_{dsim} versus RMSE = 0.22 for regional P_{dsim}) is evidence that there is limited opportunity to better reproduce the variance in debris-flow likelihood inside a fire perimeter because the fire-specific P_{dsim} is already tuned to a value that minimizes basin debris-flow likelihood RMSE. In other words, the fire-specific P_{dsim} calibration already produced the best match between simulated and observed basin debris-flow likelihood.

In regions with lower RMSE, we have higher confidence in our ability to predict mean debris-flow likelihood. In particular, the Modoc Plateau, Basin and Range, and Southern Deserts and the Southern Cascades produced relatively low RMSE values (0.03 and 0.04, respectively) relative to the Klamath Mountains and Central Coast Ranges,

Table 5. Summary of regional values.

Region			Calibration				Basins inside fire perimeter[A,C]						Fire-wide mean[B,C]	
	Fire area (km^2)	Total basins	Total fires	2020/2021 regional median of low-moderate BARC break	Regional P_{dsim}	Slope (°)	Observed dNBR	Simulated dNBR for regional P_{dsim}	Observed DFL	Simulated DFL for regional P_{dsim}	DFL RMSE for fire-specific P_{dsim}	DFL RMSE for regional P_{dsim}	DFL RMSE for fire-specific P_{dsim}	DFL RMSE for regional P_{dsim}
Central Coast Ranges	2888	4445	8	350	0.56	23.9	352	342	0.41	0.33	0.24	0.26	0.05	0.18
Klamath Mountains	4254	7059	12	321	0.40	26.2	391	326	0.44	0.41	0.29	0.33	0.02	0.13
Modoc Plateau/ Basin and Range/ Southern Deserts	1280	1891	11	272	0.38	14.7	229	231	0.19	0.20	0.11	0.11	0.00	0.03
Northern Coast Ranges	6618	9618	7	316	0.47	22.1	375	347	0.41	0.41	0.24	0.24	0.01	0.07
Northern Sierra Nevada	6982	12,782	9	312	0.49	18.5	422	356	0.41	0.39	0.22	0.22	0.00	0.07
Southern Cascades	5025	7802	5	315	0.52	15.0	378	366	0.34	0.35	0.20	0.20	0.00	0.04
Southern Sierra Nevada	3721	6243	15	310	0.40	20.4	315	308	0.27	0.25	0.19	0.20	0.01	0.08
Transverse and Peninsular Ranges	1269	1939	14	332	0.55	24.5	313	335	0.33	0.31	0.19	0.19	0.03	0.08
Regional mean	4005	6472	10	316	0.47	20.7	347	326	0.35	0.33	0.21	0.22	0.02	0.09

Abbreviations: BARC, Burned Area Reflectance Classification; DFL, debris-flow likelihood; dNBR, differenced Normalized Burn Ratio; RMSE, Root Mean Square Error.

[A]For each region, basins inside fire perimeter values were calculated as the mean value for all calibration fire basin values in the region (for example, the mean RMSE of 4445 basins in the Central Coast Ranges).

[B]Fire-wide mean values were calculated from the mean value for each calibration fire in the region (for example, the mean RMSE of 8 fire values for the Central Coast Ranges).

[C]In both cases, basins with observed dNBR less than or equal to the unburned-low BARC break (T_{low}) were excluded from the calculations.

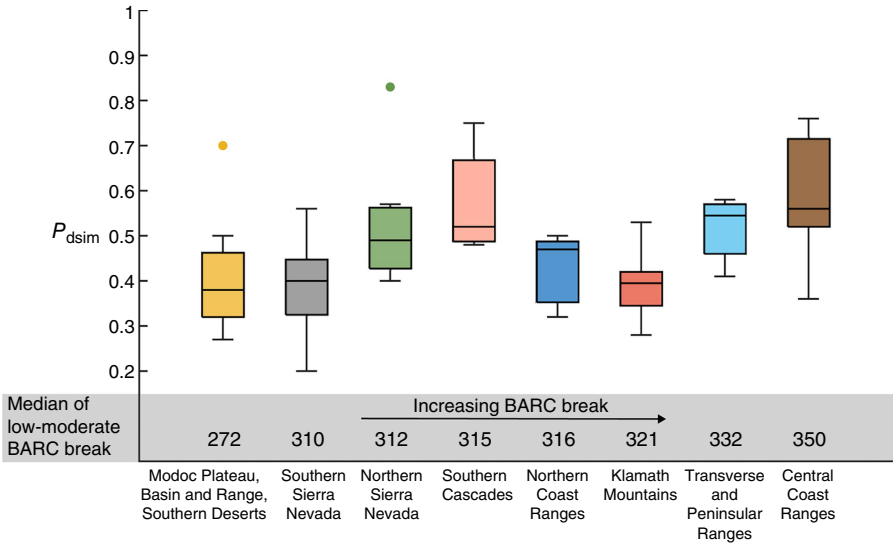

Fig. 8. Box and whisker plots summarizing distributions of fire-wide P_{dsim} values by region with increasing Burned Area Reflectance Classification (BARC) breaks for the lowest Root Mean Square Error (RMSE) method. Outliers shown as circular markers.

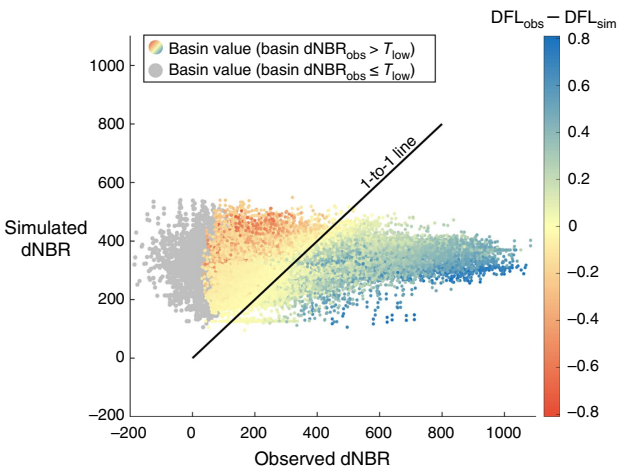

Fig. 9. Comparison of simulated and observed mean differenced Normalized Burn Ratio (dNBR) values for all calibration fire basins. Color shows the difference in the observed and simulated mean basin debris-flow likelihoods (DFL_{obs} and DFL_{sim}, respectively). Basin values with observed dNBR less than the fire-specific unburned-low Burned Area Reflectance Classification (BARC) break (T_{low}) are shown in gray. The difference between DFL_{obs} and DFL_{sim} are typically smallest near the 1-to-1 line. Nash-Sutcliffe Efficiency (NSE, 0.02) calculated for simulated and observed dNBR for basin $dNBR_{obs} > T_{low}$.

which produced relatively high RMSE values (0.13 and 0.18, respectively; Fig. 7).

Recommendations on applying the debris-flow likelihood results

The maps and associated data can be used to identify potential postfire hazards for individual basins as a function of debris-flow likelihood, volume, combined hazard classification, or annual probability of postfire debris flow. These maps can be used to prioritize treatments such as fuel reduction projects to decrease the spatial extent and severity of wildfire; prioritize road maintenance and crossing upgrades to minimize road failures and improve access for public travel, commerce, and emergency services; inform operational plans during active fire suppression activities, especially in basins with a high debris-flow hazard where there are downstream values at risk present. The results can also provide an additional, objective metric to rank basins and watersheds in comprehensive hazard assessments. For example, postfire debris-flow combined hazard classification and annual probability could be applied to identify and rank areas where modeling of debris-flow inundation would support the development of state and local hazard mitigation plans that comply with the Federal Disaster Mitigation Act (2000).

Limitations on applying the debris-flow likelihood results

Fire behavior is highly variable, and we were unable to accurately predict burn severity for individual basins in most cases (Fig. 9). However, we were somewhat successful at predicting the mean debris-flow likelihood even when using a regional P_{dsim} value (Fig. 7). Our results of predicted debris-flow likelihood represent a simplified scenario in which burn severity is controlled by vegetation type only. Using EVT to predict dNBR does help capture some variability observed in fire behavior but is limited by our inability to account for other factors that drive fire behavior. Simulated dNBR and the corresponding Burned Area Reflectance Classification (BARC) maps can be used to identify basins with high debris-flow likelihood under a simplified wildfire scenario that depends solely on EVT. Since fire behavior is difficult to predict, this simplified scenario is best at identifying areas that are naturally more prone to debris flows due to hillslope gradient, soil characteristics (through Kf factor),

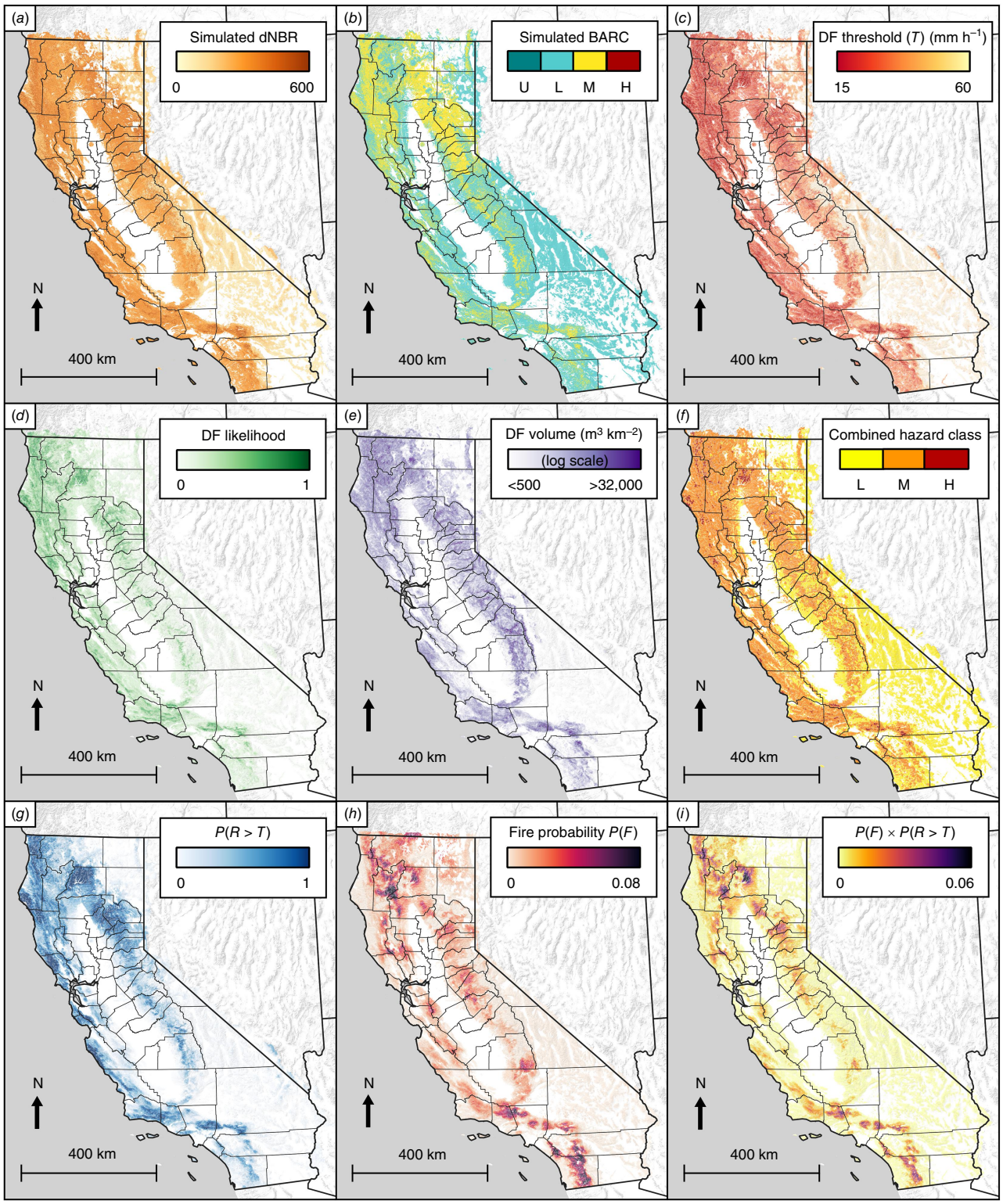

Fig. 10. Statewide prefire modeling results showing simulated differenced Normalized Burn Ratio (dNBR) (*a*), simulated Burned Area Reflectance Classification (BARC); unburned/very low (U), low (L), moderate (M), and high (H) burn severity (*b*), debris-flow (DF) 15-min rainfall intensity threshold (*T*) (*c*), debris-flow likelihood from 24 mm h^{-1} storm (*d*), debris-flow volume (normalized to basin area); (*e*), debris-flow combined hazard class; L: low, M: moderate, and H: high (*f*), annual probability that the 15-min triggering rainfall intensity is exceeded for a debris-flow likelihood value of 50% ($P(R > T)$; *g*), annual fire probability ($P(F)$; *h*), and annual probability of a fire and subsequent above-threshold rainfall intensity within the year following fire ($P(F) \times P(R > T)$; *i*).

and regional fire behavior (via calibrated prediction of dNBR and regional BARC breaks) – all of which are known prior to the fire.

Opportunities for future work

Improving our ability to forecast where landscapes are likely to experience moderate and high burn severity would dramatically improve our ability to accurately predict debris-flow likelihood. Once rainfall intensity is accounted for, moderate and high burn severity in conjunction with slope gradient are the most important factors influencing the occurrence of debris flows (Staley *et al.* 2017). There are likely opportunities to better predict burn severity and debris-flow likelihood using machine learning and other techniques. Although machine learning has been applied to many fire-related investigations, there have been relatively few attempts to use machine learning to predict fire severity (Jain *et al.* 2020; Klimas *et al.* 2025). Fire behavior and effects are fundamentally difficult to predict and the few existing attempts to use machine learning have been limited in their ability to accurately predict burn severity, especially for fires on which the model was not trained (e.g. Birch *et al.* 2015; Kane *et al.* 2015; Wells *et al.* 2023). Conditions immediately prior to the fire such as daily fire weather (air temperature, wind speed and direction, relative humidity, etc.) and fuel moisture are critical drivers of fire behavior (e.g. van Mantgem *et al.* 2013; Zald and Dunn 2018) and cannot be known far in advance; these limitations hamper our ability to incorporate critical factors into a postfire debris-flow likelihood prediction prior to wildfire. However, other important factors such as topography (elevation; aspect; landscape location – hillslope, ridge, riparian), proximity to developed areas, road density, fuel loads, rock type, and seasonal climatic information can be considered prior to fire occurrence. Indeed, some of these factors have been investigated with machine learning. Zald and Dunn (2018) used a random forest ensemble model and determined that daily fire weather was the most important predictor variable followed by stand age, ownership, and topographic position in an area impacted by the 2013 Douglas Complex Fire in southern Oregon. Wells *et al.* (2023) found that fuel loads and conditions (e.g. leaf-on chlorophyll content), prefire weather, and topography were important predictors of burn severity for two fires in north-central Colorado. Klimas *et al.* (2025) used a machine learning model and found that vegetation productivity, elevation, and canopy fuels were the most important predictor variables in forested land in Utah. Further development of machine learning approaches and other methods to estimate fire severity are promising to improve postfire debris-flow likelihood predictions prior to wildfire.

Although our goal was to assess potential debris-flow hazards for all of California, some caution should be applied when using the debris-flow likelihood and volume models (Table 1) in areas outside the original calibration area in Southern California. For example, debris-flow sediment sourcing (dry ravel, landslide, in-channel storage, hillslope rilling), sediment characteristics (grain size, shape, volume of available sediment, etc.), storm behavior (convective, atmospheric river, etc.) vary in California. These differences are currently not accounted for in the debris-flow likelihood and volume models, even though they may produce different debris-flow behavior and characteristics. An expanded database of debris-flow triggering conditions and volume is required to fully validate the models for all of California. These data are currently being collected and we expect that future versions of the debris-flow likelihood and volume models will include these data in their development.

Additionally, we note that the goals and methods of this study relate to the prediction of postfire debris-flow hazard prior to a hypothetical future fire. As such, any predictions produced as part of this study that lie within recently burned areas reflect the debris-flow likelihood that may be induced by the simulated burning of vegetation that may not represent actual postfire conditions. To assess the current debris-flow hazard in recently burned areas, we recommend consulting the USGS hazard assessment produced using observed and field-verified burn severity maps (http://landslides.usgs.gov/hazards/postfire_debrisflow). Similarly, as the data products used in our modeling approach are current as of August 2022, changes in EVT and/or fire probability that have occurred after that date (likely by recent fire) are not reflected in our model output.

Additional limitations of this study are outlined below. The climate products from NOAA Atlas14, though currently the most comprehensive estimate of rainfall-intensity climatology in the study area, quantify only the past climatology in the area rather than future climate. As a result, they may not capture changes in rainfall climatology that may result from an ongoing climate change. Additionally, many of the gage records used in the computation of the Atlas14 product are less than 50 years in duration, meaning that the 50-year 15-min product is based on extrapolation rather than true quantification of the 50-year recurrence interval storm. Furthermore, the link between drought and short-duration rainfall intensities important for runoff-generated debris-flow occurrence is poorly understood and provides an opportunity for future climate modeling work that may improve prefire predictions.

The FSim fire probability product also has several limitations. Similar to Atlas14, the weather component of the fire probability simulation is based on past climate records rather than future climate predictions. The model is also calibrated only on fires >100 ha in size, though the authors acknowledge that the role of fires smaller than this threshold on overall fire probability is likely negligible. Also, the latest statewide release of FSim is valid from August 2022, so the decreases in future fire probability present in areas burned between August 2022 and the release of this study are not captured in our products.

Conclusion

We presented a consistent methodology to model postfire debris-flow hazards in California prior to wildfire using simulated differenced Normalized Burn Ratio (dNBR) data calibrated from 2020 to 2021 fire data, NOAA Atlas 14 rainfall data, and fire probability data developed by Pyrologix. The dNBR and other data were used to predict debris-flow likelihood and volume for a 15-min rainfall intensity of 24 mm h^{-1}. The largest source of uncertainty in predicting postfire debris-flow likelihood and volume is due to the difficulty in predicting dNBR, a proxy for soil burn severity, prior to wildfire. Our approach tended to produce regionally consistent simulated dNBR while actual fires will produce a wider range in dNBR. Some areas will experience lower burn severity while other areas will experience higher burn severity. Areas that burn at high soil burn severity will experience higher debris-flow likelihood relative to debris-flow likelihoods presented here. Because the debris-flow likelihood and volume predictions are for a fixed rainfall intensity and assume that a fire has occurred, we also calculated the annual probability that a wildfire and the 15-min triggering rainfall intensity for a debris-flow likelihood of 50% will occur using NOAA Atlas14 rainfall recurrence data, the debris-flow likelihood model, and the Pyrologix fire probability product. This debris-flow product can be used to identify regions that are most likely to experience postfire debris flows. Once these regions are identified, our debris-flow likelihood and volume products can be used to target specific basins that would benefit from prefire mitigation efforts, such as improvements to stream crossings. Ultimately, these products of postfire debris-flow prediction prior to wildfire should aid prefire efforts to mitigate debris-flow risks.

References

Barnhart KR, Jones RP, George DL, McArdell BW, Rengers FK, Staley DM, Kean JW (2021) Multi-model comparison of computed debris flow runout for the 9 January 2018 Montecito, California post-wildfire event. *Journal of Geophysical Research: Earth Surface* **126**(12), e2021JF006245. doi:10.1029/2021JF006245

Belongia MF, Hammond Wagner C, Seipp KQ, Ajami NK (2023) Building water resilience in the face of cascading wildfire risks. *Science Advances* **9**(37), eadf9534. doi:10.1126/sciadv.adf9534

Birch DS, Morgan P, Kolden CA, Abatzoglou JT, Dillon GK, Hudak AT, Smith AM (2015) Vegetation, topography and daily weather influenced burn severity in central Idaho and western Montana forests. *Ecosphere* **6**(1), 1–23. doi:10.1890/ES14-00213.1

California Department of Forestry and Fire Protection (2024) Statistics. Available at https://www.fire.ca.gov/our-impact/statistics [accessed 7 May 2024]

California Geological Survey (1997) 'California Geomorphic Provinces'. Note 36. (California Division of Mines and Geology)

Cannon S, Gartner JR, Michael J, Rea A, Parrett C (2010) Predicting the probability and volume of post-wildfire debris flows in the intermountain west, USA. *Geological Society of America Bulletin* **122**(1/2), 127–144. doi:10.1130/B26459.1

Disaster Mitigation Act (2000) Public Law 106-390. 114 Stat. 1552.

Estes BL, Knapp EE, Skinner CN, Miller JD, Preisler HK (2017) Factors influencing fire severity under moderate burning conditions in the Klamath Mountains, northern California, USA. *Ecosphere* **8**(5), e01794. doi:10.1002/ecs2.1794

Feller W (1991) 'An introduction to probability theory and its applications.' Vol. 2(81). (John Wiley and Sons)

Gartner JE, Cannon SH, Santi PM (2014) Empirical models for predicting volumes of sediment deposited by debris flows and sediment-laden floods in the transverse ranges of southern California. *Engineering Geology* **176**, 45–56. doi:10.1016/j.enggeo.2014.04.008

Jain P, Coogan SC, Subramanian SG, Crowley M, Taylor S, Flannigan MD (2020) A review of machine learning applications in wildfire science and management. *Environmental Reviews* **28**(4), 478–505. doi:10.1139/er-2020-0019

Kane VR, Cansler CA, Povak NA, Kane JT, McGaughey RJ, Lutz JA, Churchill DJ, North MP (2015) Mixed severity fire effects within the Rim fire: relative importance of local climate, fire weather, topography, and forest structure. *Forest Ecology and Management* **358**, 62–79. doi:10.1016/j.foreco.2015.09.001

Kean JW, Staley DM (2021) Forecasting the frequency and magnitude of postfire debris flows across southern California. *Earth's Future* **9**(3), e2020EF001735. doi:10.1029/2020EF001735

Kean JW, Staley DM, Cannon SH (2011) In situ measurements of postfire debris flows in southern California: comparisons of the timing and magnitude of 24 debris-flow events with rainfall and soil moisture conditions. *Journal of Geophysical Research: Earth Surface* **116**(F4), F04019. doi:10.1029/2011JF002005

Kean JW, Staley DM, Lancaster JT, Rengers FK, Swanson BJ, Coe JA, Hernandez JL, Sigman AJ, Allstadt KE, Lindsay DN (2019) Inundation, flow dynamics, and damage in the 9 January 2018 Montecito debris-flow event, California, USA: opportunities and challenges for post-wildfire risk assessment. *Geosphere* **15**(4), 1140–1163. doi:10.1130/GES02048.1

King J (2023) pfdf - Python library for postfire debris-flow hazard assessments and research, version 1.1.0: U.S. Geological Survey software release. doi:10.5066/P13RSBEE

Klimas KB, Yocom LL, Murphy BP, David SR, Belmont P, Lutz JA, DeRose RJ, Wall SA (2025) A machine learning model to predict wildfire burn severity for pre-fire risk assessments, Utah, USA. *Fire Ecology* **21**, 8. doi:10.1186/s42408-024-00346-z

LandFire (2022) Existing vegetation type. Available at https://www.landfire.gov/index.php [accessed 29 March 2024]

Li S, Banerjee T (2021) Spatial and temporal pattern of wildfires in California from 2000 to 2019. *Scientific Reports* **11**(1), 8779. doi:10.1038/s41598-021-88131-9

MTBS (2022) Monitoring Trends in Burn Severity. Burned Areas Boundaries Dataset. Available at https://www.mtbs.gov/direct-download [accessed 29 March 2024]

Parsons A, Robichaud PR, Lewis SA, Napper C, Clark JT (2010) 'Field guide for mapping post-fire soil burn severity.' (US Department of Agriculture, Forest Service, Rocky Mountain Research Station: Fort Collins, CO, USA)

Perica S, Dietz S, Heim S, Hiner L, Maitaria K, Martin D, Pavlovic S, Roy I, Trypaluk C, Unruh D, Yan F (2014) 'NOAA Atlas 14, precipitation-frequency Atlas of the United States, 6 (Version 2.3) [California].' (National Oceanic and Atmospheric Administration: Silver Spring, MD) Available at https://hdsc.nws.noaa.gov/hdsc/pfds/index.html [accessed 29 March 2024]

Radeloff VC, Helmers DP, Kramer HA, Mockrin MH, Alexandre PM, Bar-Massada A, Butsic V, Hawbaker TJ, Martinuzzi S, Syphard AD, Stewart SI (2018) Rapid growth of the US wildland-urban interface raises wildfire risk. *Proceedings of the National Academy of Sciences* **115**(13), 3314–3319. doi:10.1073/pnas.1718850115

Rossi RK, Richardson PW, Cavagnaro DB, Lukashov SG, Miller ME, Lindsay DN (2025) Predicting potential postfire debris-flow hazards across California prior to wildfire [Dataset]. Zenodo. doi:10.5281/zenodo.15313560

Rundio DE, Spence BC, Chase DM, Ostberg CO (2024) Using environmental DNA to assess the response of steelhead/Rainbow Trout and Coastrange Sculpin populations to postfire debris flows in coastal streams of Big Sur, California. *North American Journal of Fisheries Management* **44**, 1167–1182. doi:10.1002/nafm.11032

Schwartz GE, Alexander RB (1995) Soils data for the conterminous United States derived from the NRCS State Soil Geographic (STATSGO) Database: U.S. Geological Survey Open-File Report 95-449. Available at https://water.usgs.gov/GIS/metadata/usgswrd/XML/ussoils.xml [accessed 29 March 2024]

Staley DM (2018) Data used to characterize the historical distribution of wildfire severity in the western United States in support of pre-fire assessment of debris-flow hazards: US Geological Survey Data Release. doi:10.5066/P9TKYL5K

Staley DM, Kean JW, Cannon SH, Schmidt KM, Laber JL (2013) Objective definition of rainfall intensity–duration thresholds for the initiation of post-fire debris flows in southern California. *Landslides* **10**, 547–562. doi:10.1007/S10346-012-0341-9

Staley DM, Negri JA, Kean JW, Laber JL, Tillery AC, Youberg AM (2016) Updated logistic regression equations for the calculation of post-fire debris-flow likelihood in the western United States. US Geological Survey Open-File Report 2016–1106. doi:10.3133/ofr20161106

Staley DM, Negri JA, Kean JW, Laber JL, Tillery AC, Youberg AM (2017) Prediction of spatially explicit rainfall intensity–duration thresholds for post-fire debris-flow generation in the western United States. *Geomorphology* **278**, 149–162. doi:10.1016/j.geomorph.2016.10.019

Staley DM, Tillery AC, Kean JW, McGuire LA, Pauling HE, Rengers FK, Smith JB (2018) Estimating post-fire debris-flow hazards prior to wildfire using a statistical analysis of historical distributions of fire severity from remote sensing data. *International Journal of Wildland Fire* **27**(9), 595–608. doi:10.1071/WF17122

Staley DM, Kean JW, Rengers FK (2020) The recurrence interval of post-fire debris-flow generating rainfall in the southwestern United States. *Geomorphology* **370**, 107392. doi:10.1016/j.geomorph.2020.107392

Swanson BJ, Lindsay DN, Cato K, DiBiase RA, Neely AB (2024) Debris flows and sediment transport at Yucaipa Ridge and impacts to Oak Glen and Forest Falls area, southern California, following the 2020 El Dorado and Apple Fires. In 'From Coastal Geomorphology to Magmatism: Guides to GSA Connects 2024 Field Trips in Southern California and Beyond'. Geological Society of America Field Guide 70. (Eds NJ Van Buer, JJ Schwartz) pp. 45–73. (Geological Society of America) doi:10.1130/2024.0070(03)

Thomas MA, Lindsay DN, Cavagnaro DB, Kean JW, McCoy SW, Graber AP (2023) The rainfall intensity-duration control of debris flows after wildfire. *Geophysical Research Letters* **50**, e2023GL103645. doi:10.1029/2023GL103645

US Forest Service (2009) 'Existing Vegetation – CALVEG.' (USDA-Forest Service, Pacific Southwest Region) Available at https://www.fs.usda.gov/detail/r5/landmanagement/resourcemanagement/ [accessed 29 March 2024]

US Forest Service (2023) The future of fires with FSim: projecting future climate-altered fire regimes using FSim. Available at https://www.fs.usda.gov/research/sites/default/files/2023-11/fsim-fact-sheet-110823.pdf [accessed 10 June 2024]

US Geological Survey (2020) National Hydrography Dataset (NHD) 20200619 for California State or Territory FileGDB 10.1 (Version 2.2.1) [Waterbodies]. [accessed 29 March 2024]

US Geological Survey (2023) Watershed Boundary Dataset (WBD) 20231127 FileGDB – Hydrologic Unit (HU) 8/10. [accessed on 29 March 2024]

US Geological Survey (2024) 3D Elevation Program 10-Meter Resolution Digital Elevation Model [USGS 1/3 Arc Second]. Available at https://apps.nationalmap.gov/downloader/ [accessed 29 March 2024]

van Mantgem PJ, Nesmith JC, Keifer M, Knapp EE, Flint A, Flint L (2013) Climatic stress increases forest fire severity across the western United States. *Ecology Letters* **16**(9), 1151–1156. doi:10.1111/ele.12151

Vogler KC, Brough A, Moran CJ, Scott JH, Gilbertson-Day JW (2021) 'Contemporary wildfire hazard across California.' (Pyrologix, LLC)

Wells AG, Hawbaker TJ, Hiers JK, Kean JW, Loehman RA, Steblein PF (2023) Predicting burn severity for integration with post-fire debris-flow hazard assessment: a case study from the Upper Colorado River Basin, USA. *International Journal of Wildland Fire* **32**(9), 1315–1331. doi:10.1071/WF22200

Zald H, Dunn CJ (2018) Severe fire weather and intensive forest management increase fire severity in a multi-ownership landscape. *Ecological Applications* **28**(4), 1068–1080. doi:10.1002/eap.1710

Zekkos D, Stark TD (2023) 'Highway 1 Rat Creek Embankment Failure'. Geotechnical Special Publication No. 337. (American Society of Civil Engineers) doi:10.1061/9780784484579

Data availability. Data associated with this manuscript are available at an online repository (Rossi *et al.* 2025).

Conflicts of interest. The authors declare that they have no conflicts of interest.

Declaration of funding. This study was funded by the California Geological Survey.

Acknowledgements. We thank Jason Kean and Jonathan King (USGS) for providing comments on earlier drafts of the manuscript, postfire debris-flow hazard assessment examples, and support of the pfdf Python library.

Author affiliations

[A]California Geological Survey, Burned Watershed Geohazards Program, Sacramento, CA 95814, USA.

[B]California Geological Survey, Burned Watershed Geohazards Program, Redding, CA 96002, USA.

[C]Michigan Technological University, Michigan Tech Research Institute, Ann Arbor, MI 48105, USA.